
Neural Networks Loss Landscape Convergence in Hessian Low-Dimensional Space

Tem Nikitin

Moscow Institute of Physics and Technology
Moscow, Russia
nikitin.artem.a@phystech.su

Nikita Kiselev

Moscow Institute of Physics and Technology
Moscow, Russia
kiselev.ns@phystech.su

Andrey Grabovoy

Moscow Institute of Physics and Technology
Moscow, Russia
grabovoy.av@phystech.su

Vladislav Meshkov

Moscow Institute of Physics and Technology
Moscow, Russia
meshkov.ns@phystech.su

Abstract

Understanding how a neural network’s loss landscape changes as we add more training data is important for efficient training. Although larger datasets are known to reshape this high-dimensional surface, the point when extra data stop making a big difference is still unclear.

In this paper, we study this issue and show that the loss landscape near a local minimum stabilizes once the dataset exceeds a certain size. To analyze this, we project the full parameter space onto a smaller subspace formed by the Hessian’s top eigenvectors. This low-dimensional view highlights how the loss surface changes in its most important directions. We then apply Monte Carlo sampling within this subspace to estimate these changes more precisely.

We test our approach on standard image-classification tasks and find that our low-dimensional analysis pinpoints when the landscape stops evolving. These findings clarify how dataset size affects optimization and offer practical guidance for balancing training cost with performance gains.

Keywords: Neural networks, Loss landscape, Low-dimensional subspace, Hessian eigenvectors, Monte Carlo estimation, Dataset size threshold.

1 Introduction

Neural networks are now essential in many areas — image classification, language modeling, recommender systems, and more. As models and datasets grow, we often see better accuracy and new breakthroughs. But bigger networks and data also demand more computation time and resources, which can become prohibitive. While prior work has compared various optimization methods under fixed data and model sizes [1], the question of when adding more training samples stops yielding significant gains remains largely unanswered.

In this paper, we investigate exactly that: how the loss landscape changes as we increase the dataset size, and at what point further data have little effect. Knowing this “minimum viable dataset size” — a threshold beyond which new samples bring negligible improvement — can save both training time and data-collection effort. We also relate this threshold to generalization behavior, along the lines of [2].

To study this, we use the Hessian of the loss function as a proxy for local curvature. Computing the full Hessian is expensive, so we project the parameter space onto a low-dimensional subspace formed by its top eigenvectors. Our main contributions are:

1. Constructing a Hessian-based projection that captures the principal curvature directions.
2. Applying Monte Carlo and other sampling methods to identify when the loss landscape stabilizes as dataset size grows.
3. Visualizing the projected loss surface around local minima to illustrate these changes.
4. Deriving theoretical criteria — using results from The Matrix Cookbook [3] — to predict when additional samples have minimal impact.

This approach is novel in linking low-rank Hessian estimation to a concrete dataset threshold, enabling more cost-effective data collection and a clearer understanding of how data scale interacts with loss geometry. We validate our method on MNIST [4] and Fashion-MNIST [5], demonstrating how to balance computational cost against accuracy gains.

Organization. The rest of the paper is structured as follows. Section 2 reviews related work. Section 3 introduces notation and preliminaries. Section 4 derives theoretical bounds on Hessian spectra and the loss-difference norm. Section 5 presents our empirical studies. We discuss the implications in Section 6 and conclude in Section 7. Additional experiments and proofs are provided in Appendix A.

2 Related Work

Hessian-based Analysis. The loss landscape of neural networks has been extensively studied using Hessian-based techniques, which illuminate convergence behavior and curvature properties [6]. Empirical work shows that near local minima the Hessian often has low effective rank, indicating a small "active subspace" spanned by a few large eigenvalues [7]. Ghorbani et al. [8] examined how these large eigenvalues emerge during training and shape optimization dynamics. Meshkov et al. [9] extended this analysis to fully connected and convolutional architectures, though broader validation across architectures remains an open challenge.

Loss Landscape Geometry and Dataset Size. Another research direction explores how dataset size influences model performance and landscape geometry. Networks trained on larger datasets tend to find flatter, wider minima that generalize better [2]. Yet, acquiring and processing massive data is costly, motivating studies of optimal data–model trade-offs [10]. Li et al. [11] developed visualization tools that reveal how dataset size, initialization, and architecture affect the topology of loss surfaces.

Algorithmic Stability and Landscape Sensitivity. Algorithmic stability, which measures how small changes in the training set affect the learned model, provides theoretical bounds on generalization error [12]. Elisseeff et al. [13] extended stability analysis to randomized algorithms such as bagging and ensemble methods, deriving non-asymptotic generalization guarantees. In our context, stability theory underpins the intuition that, beyond a certain dataset size, further samples cause negligible changes to the loss curvature. Our Monte Carlo–based Hessian projection method directly leverages this perspective, using top eigenvectors to quantify and visualize when the loss landscape stabilizes as new data are added.

3 Preliminaries

3.1 General notation

We consider a K -class classification problem. Let $\mathbf{x} \in \mathbf{X}$ be an input and $y \in \mathcal{Y} = \{1, \dots, K\}$ its label. A neural network with parameters $\mathbf{w} \in \Omega \subset \mathbb{R}^P$ defines a mapping $f_{\mathbf{w}} : \mathbf{X} \rightarrow \mathbb{R}^K$. Given a dataset

$$\mathcal{D} = \{(\mathbf{x}_i, y_i)\}_{i=1}^m$$

of m i.i.d. samples, and a per-sample loss $\ell(f_{\mathbf{w}}(\mathbf{x}_i), y_i)$ (e.g. cross-entropy), we define

$$\ell_i(\mathbf{w}) = \ell(f_{\mathbf{w}}(\mathbf{x}_i), y_i).$$

Definition 1. The empirical loss on the first k samples is

$$\mathcal{L}_k(\mathbf{w}) = \frac{1}{k} \sum_{i=1}^k \ell_i(\mathbf{w}),$$

so that the full-sample loss is $\mathcal{L}(\mathbf{w}) = \mathcal{L}_m(\mathbf{w})$.

A simple telescoping gives the difference

$$\mathcal{L}_{k+1}(\mathbf{w}) - \mathcal{L}_k(\mathbf{w}) = \frac{\ell_{k+1}(\mathbf{w}) - \mathcal{L}_k(\mathbf{w})}{k+1}.$$

Definition 2. The Hessian of \mathcal{L}_k at \mathbf{w} is

$$\mathbf{H}_k(\mathbf{w}) = \nabla_{\mathbf{w}}^2 \mathcal{L}_k(\mathbf{w}) = \frac{1}{k} \sum_{i=1}^k \nabla_{\mathbf{w}}^2 \ell_i(\mathbf{w}),$$

and, similarly, the full-sample Hessian is $\mathbf{H}(\mathbf{w}) = \mathbf{H}_m(\mathbf{w}) = \nabla_{\mathbf{w}}^2 \mathcal{L}_m(\mathbf{w})$.

To capture the overall change in the landscape when adding one more sample, we introduce a Δ -function:

Definition 3. Let $p(\mathbf{w})$ be a weighting (e.g. peaked near a local minimum). Define

$$\Delta_k = \int (\mathcal{L}_{k+1}(\mathbf{w}) - \mathcal{L}_k(\mathbf{w}))^2 p(\mathbf{w}) d\mathbf{w}.$$

We study the behavior of Δ_k as $k \rightarrow \infty$ and define a threshold:

Definition 4. Fix a tolerance $\Delta > 0$. The sufficient sample size is

$$k^* = \inf\{k \mid \forall m \geq k : \Delta_m < \Delta\}.$$

When $k \geq k^*$, adding further samples changes the loss landscape by less than Δ .

3.2 Assumptions

We make the following standard assumptions to simplify our analysis around a local minimizer \mathbf{w}^* .

Assumption 1. The point \mathbf{w}^* is a common local minimizer for both \mathcal{L}_k and \mathcal{L}_{k+1} , i.e.

$$\nabla \mathcal{L}_k(\mathbf{w}^*) = \nabla \mathcal{L}_{k+1}(\mathbf{w}^*) = 0.$$

Under this assumption, a second-order Taylor expansion of \mathcal{L}_k about \mathbf{w}^* gives

$$\mathcal{L}_k(\mathbf{w}) \approx \mathcal{L}_k(\mathbf{w}^*) + \frac{1}{2} (\mathbf{w} - \mathbf{w}^*)^\top \mathbf{H}_k(\mathbf{w}^*) (\mathbf{w} - \mathbf{w}^*).$$

Assumption 2. At the minimizer \mathbf{w}^* , the loss values for consecutive sample sizes are the same:

$$\mathcal{L}_{k+1}(\mathbf{w}^*) = \mathcal{L}_k(\mathbf{w}^*).$$

Assumption 3. The parameters \mathbf{w} are distributed according to a density $p(\mathbf{w})$ (e.g. a Gaussian prior centered at \mathbf{w}^*). Then

$$\Delta_k = \int (\mathcal{L}_{k+1}(\mathbf{w}) - \mathcal{L}_k(\mathbf{w}))^2 p(\mathbf{w}) d\mathbf{w} = \mathbb{E}_{p(\mathbf{w})} (\mathcal{L}_{k+1}(\mathbf{w}) - \mathcal{L}_k(\mathbf{w}))^2 =$$

$$\mathbb{D}_{p(\mathbf{w})} [\mathcal{L}_{k+1}(\mathbf{w}) - \mathcal{L}_k(\mathbf{w})] + \left(\mathbb{E}_{p(\mathbf{w})} [\mathcal{L}_{k+1}(\mathbf{w}) - \mathcal{L}_k(\mathbf{w})] \right)^2.$$

4 Method: Projection onto Dominant Eigen-Directions and Loss Landscape Approximation

Working with the full Hessian $\mathbf{H}_k(\mathbf{w})$ of a neural network is computationally expensive due to the high dimensionality of the parameter space Ω . To reduce this cost, we project the parameters onto a lower-dimensional subspace spanned by the d dominant eigenvectors of the Hessian at a local minimum \mathbf{w}^* .

The justification for this projection is that, empirically, the Hessian has low effective rank near a minima [7]: only a few eigenvalues are significantly above zero, while the rest are negligible. Therefore, directions corresponding to small eigenvalues contribute little to loss variation. Retaining only the top d eigenvectors yields a compact yet informative representation of the most important curvature directions.

For illustration, Figure 1 plots the top few eigenvalues of $\mathbf{H}(\mathbf{w}^*)$ in descending order. We compute these dominant eigenvalues using the iterative power-method described at [14].

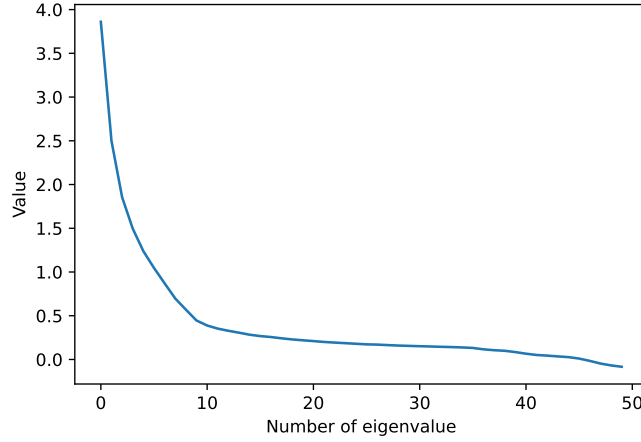


Figure 1: Top eigenvalues of $\mathbf{H}(\mathbf{w}^*)$ in descending order.

Concretely, let

$$\mathbf{P} = [\mathbf{e}_1, \dots, \mathbf{e}_d]$$

be the matrix whose columns are the top d eigenvectors. We write any parameter vector as

$$\mathbf{w} = \mathbf{w}^* + \mathbf{P} \boldsymbol{\theta}, \quad \boldsymbol{\theta} \in \mathbb{R}^d.$$

Substituting into a second-order Taylor expansion of \mathcal{L}_k around \mathbf{w}^* gives

$$\mathcal{L}_k(\mathbf{w}^* + \mathbf{P} \boldsymbol{\theta}) \approx \mathcal{L}_k(\mathbf{w}^*) + \frac{1}{2} \boldsymbol{\theta}^\top (\mathbf{P}^\top \mathbf{H}_k(\mathbf{w}^*) \mathbf{P}) \boldsymbol{\theta} = \mathcal{L}_k(\mathbf{w}^*) + \frac{1}{2} \boldsymbol{\theta}^\top \boldsymbol{\Lambda}_k \boldsymbol{\theta},$$

where

$$\boldsymbol{\Lambda}_k = \mathbf{P}^\top \mathbf{H}_k(\mathbf{w}^*) \mathbf{P} = \text{diag}(\lambda_k^1, \dots, \lambda_k^d).$$

An identical expansion holds for \mathcal{L}_{k+1} , yielding $\boldsymbol{\Lambda}_{k+1}$ from the Hessian on $k+1$ samples.

Theorem 1 (Approximate Δ_k via Eigenvalues). *Under the assumption that $\boldsymbol{\theta} \sim \mathcal{N}(0, \sigma^2 \mathbf{I}_d)$, the change in loss can be estimated by*

$$\Delta_k = \mathbb{E}[\mathcal{L}_{k+1}(\mathbf{w}) - \mathcal{L}_k(\mathbf{w})]^2 \approx \frac{\sigma^4}{4} \left(2 \sum_{i=1}^d (\lambda_{k+1}^i - \lambda_k^i)^2 + \left(\sum_{i=1}^d (\lambda_{k+1}^i - \lambda_k^i) \right)^2 \right).$$

Remark 1. Assuming $\mathbb{E}_{p(\boldsymbol{\theta})}(\boldsymbol{\theta}) = \mathbf{0}$ is natural when centering the sampling distribution at the minimum.

This formula uses only the top d eigenvalues, so it is efficient to compute even for very large models. In practice, it provides an upper bound on the empirical Δ_k and thus a reliable criterion for determining when the dataset size is sufficient.

5 Experiments

To validate our theoretical estimates, we perform a set of experiments that track how the loss landscape changes as we grow the training set.

Datasets. We evaluate on MNIST [4] and Fashion-MNIST [5], each containing 60,000 training and 10,000 test grayscale images of size 28×28 pixels.

Model Architecture. All experiments use a simple multilayer perceptron (MLP) with ReLU activations. We keep the same architecture—number of hidden layers and hidden units—across all runs to ensure a fair comparison.

Experimental Procedure.

1. **Random-direction visualization:** As an initial sanity check, we project the parameters onto two random directions and plot the resulting 3D loss landscapes and their squared differences.
2. **Hessian-based analysis:** We then repeat the visualization and compute Δ_k by projecting onto the top two (and up to $d = 10$) eigenvectors of the Hessian. This directly tests our eigenvalue-based approximation and the convergence behavior predicted by theory.

All code and detailed configuration files are available in our GitHub repository.

5.1 Preliminary Experiment: Projection onto Random Directions

5.1.1 Visualizing the Loss Landscape

To build intuition for how the loss surface changes with training-set size, we first project the model parameters onto two random directions. Specifically, we pick two random vectors $\mathbf{v}_1, \mathbf{v}_2 \in \mathbb{R}^P$ in parameter space and study the subspace they span.

We then evaluate the empirical loss

$$\mathcal{L}_k(\mathbf{w}) = \frac{1}{k} \sum_{i=1}^k \ell_i(\mathbf{w}),$$

where $\ell_i(\mathbf{w}) = \ell(f_{\mathbf{w}}(\mathbf{x}_i), y_i)$, over a grid in the (α, β) plane defined by

$$\mathbf{w}(\alpha, \beta) = \mathbf{w}^* + \alpha \mathbf{v}_1 + \beta \mathbf{v}_2, \quad (\alpha, \beta) \in [-1, 1]^2.$$

1. **Grid Sampling.** We form a uniform grid of (α, β) pairs in $[-1, 1] \times [-1, 1]$ with a fixed step size.
2. **Loss Computation.** For each (α, β) , we set $\mathbf{w} = \mathbf{w}(\alpha, \beta)$, keep the base weights \mathbf{w}^* fixed, and compute both $\mathcal{L}_k(\mathbf{w})$ and $\mathcal{L}_{k+1}(\mathbf{w})$.
3. **Aggregated Metrics.**
 - The surface $\mathcal{L}_k(\alpha, \beta)$ visualizes how the mean loss changes over the grid.
 - The surface $(\mathcal{L}_{k+1}(\alpha, \beta) - \mathcal{L}_k(\alpha, \beta))^2$ highlights where adding one sample causes the largest change.
4. **3D Visualization.** We render two side-by-side 3D plots:
 - *Left:* $\mathcal{L}_k(\alpha, \beta)$ vs. (α, β) .
 - *Right:* $(\mathcal{L}_{k+1}(\alpha, \beta) - \mathcal{L}_k(\alpha, \beta))^2$ vs. (α, β) .

Loss Landscape for Small Sample Size In Figure 2 ($k = 1$), the loss surface is highly irregular, with sharp peaks and deep valleys. This irregularity indicates that with very few training samples, the model is extremely sensitive to small parameter perturbations. The squared difference surface also exhibits large spikes, confirming that adding a single data point can cause substantial local changes in the loss.

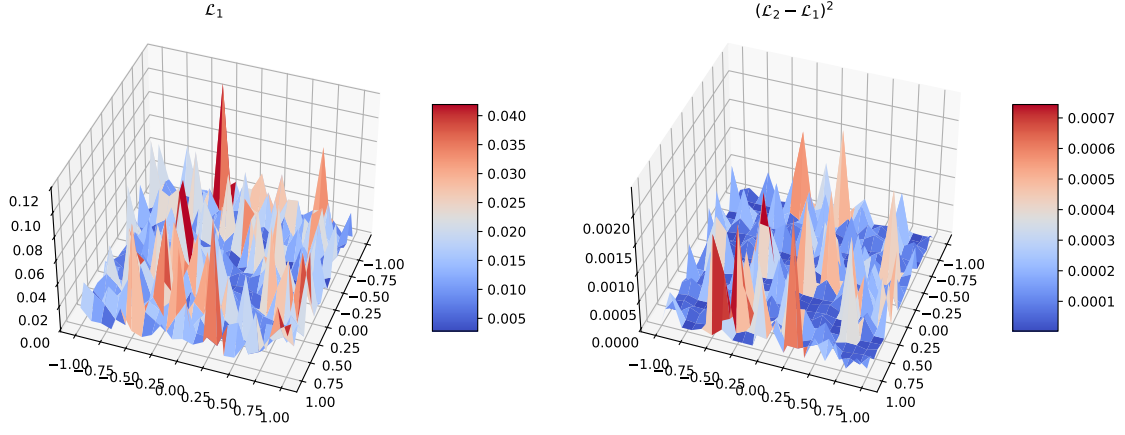


Figure 2: Loss function landscape for small k , projected onto the two random directions.

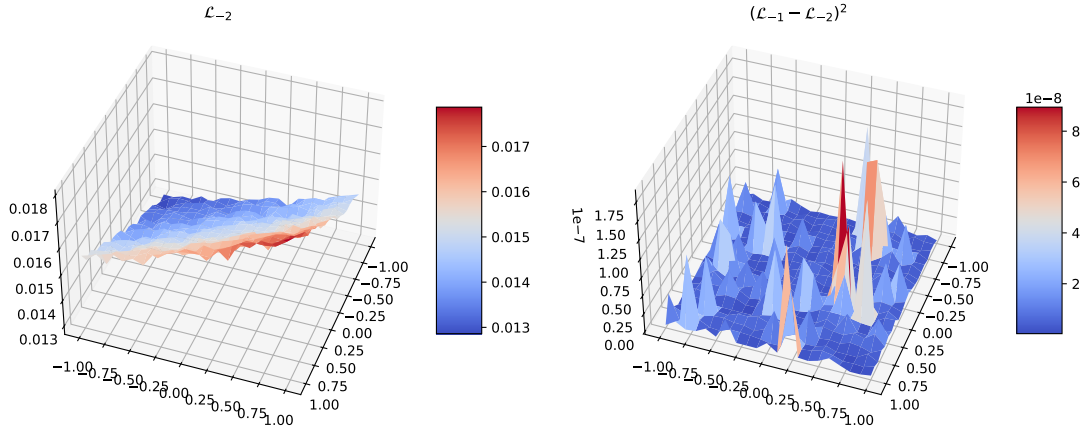


Figure 3: Loss function landscape for maximum k , projected onto the two random directions.

Loss Landscape for Maximum Dataset Size In contrast, Figure 3 (maximum k) shows a much smoother loss surface with gentle slopes. The overall loss values are lower — reflecting the averaging effect of more samples — and the squared difference surface is correspondingly much smaller. This smoothing demonstrates that as the dataset grows, the local optimum stabilizes, and additional samples produce only minor adjustments to the loss landscape. Hence, beyond a certain dataset size, further data have negligible impact on the shape of the loss surface.

5.1.2 Visualizing the Δ_k Function

To study how the loss landscape converges as the dataset grows, we estimate and plot the function

$$\Delta_k = \mathbb{E}_{p(\mathbf{w})} [\mathcal{L}_{k+1}(\mathbf{w}) - \mathcal{L}_k(\mathbf{w})]^2$$

via a Monte Carlo approximation using Gaussian perturbations in parameter space. The steps are:

1. **Sample directions.** Starting from a fixed trained model with parameters \mathbf{w}^* , draw K independent random vectors

$$\boldsymbol{\theta}^{(t)} \sim \mathcal{N}(\mathbf{0}, \sigma^2 \mathbf{I}_d), \quad t = 1, \dots, K.$$

2. **Perturb parameters.** For each sample, form a perturbed parameter set

$$\mathbf{w}^{(t)} = \mathbf{w}^* + \boldsymbol{\theta}^{(t)}.$$

3. **Evaluate loss differences.** Compute

$$\mathcal{L}_k(\mathbf{w}^{(t)}) \quad \text{and} \quad \mathcal{L}_{k+1}(\mathbf{w}^{(t)}),$$

then calculate the squared difference

$$d_t = [\mathcal{L}_{k+1}(\mathbf{w}^{(t)}) - \mathcal{L}_k(\mathbf{w}^{(t)})]^2.$$

4. **Compute Monte Carlo estimate.** Approximate

$$\Delta_k \approx \frac{1}{K} \sum_{t=1}^K d_t.$$

Increasing K reduces the variance of this estimator.

5. **Plot results.** We plot Δ_k versus k to observe its decay. We also plot the scaled quantity

$$\Delta_k \cdot k^2$$

alongside to highlight an $\mathcal{O}(1/k)$ convergence rate.

Figures 4 and 5 present the behavior of the function

$$\Delta_k = \mathbb{E} [\mathcal{L}_{k+1}(\mathbf{w}) - \mathcal{L}_k(\mathbf{w})]^2$$

under different Monte Carlo sampling settings and projection subspace sizes. Each figure isolates one variable:

- Figure 4: varying the Gaussian variance σ .
- Figure 5: varying the subspace dimension d .

Comparing Different Variances σ Figure 4 shows that varying the Gaussian variance σ produces no substantial change in the shape or magnitude of the Δ_k curves. This insensitivity likely stems from using random projection directions: since they do not align with the dominant curvature axes of the Hessian, scaling those directions has little impact on the estimated loss differences.

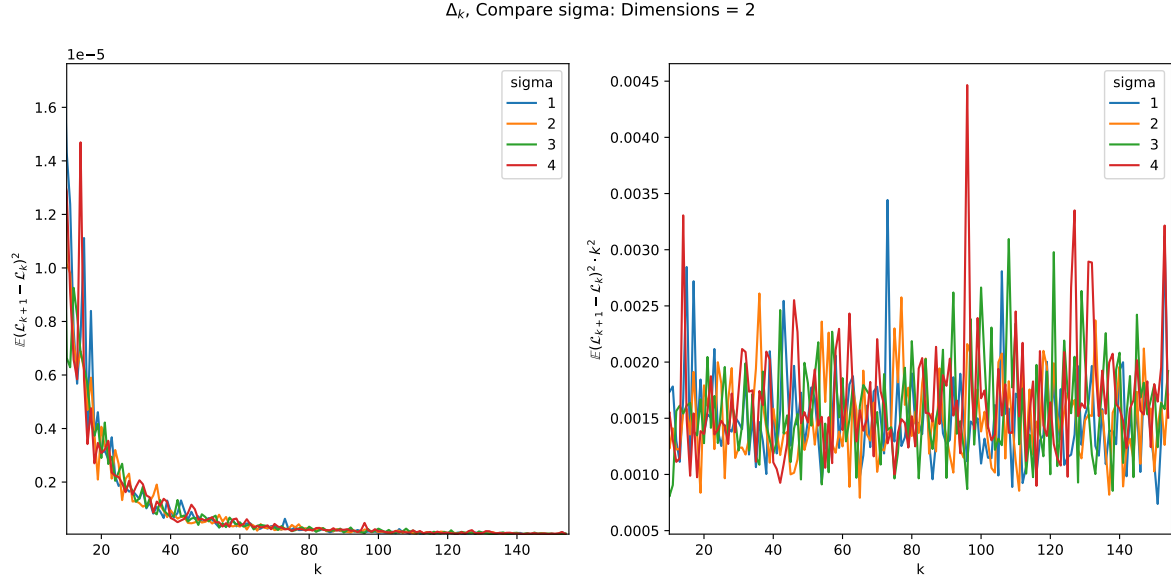


Figure 4: Delta function landscape varying the Gaussian variance σ .

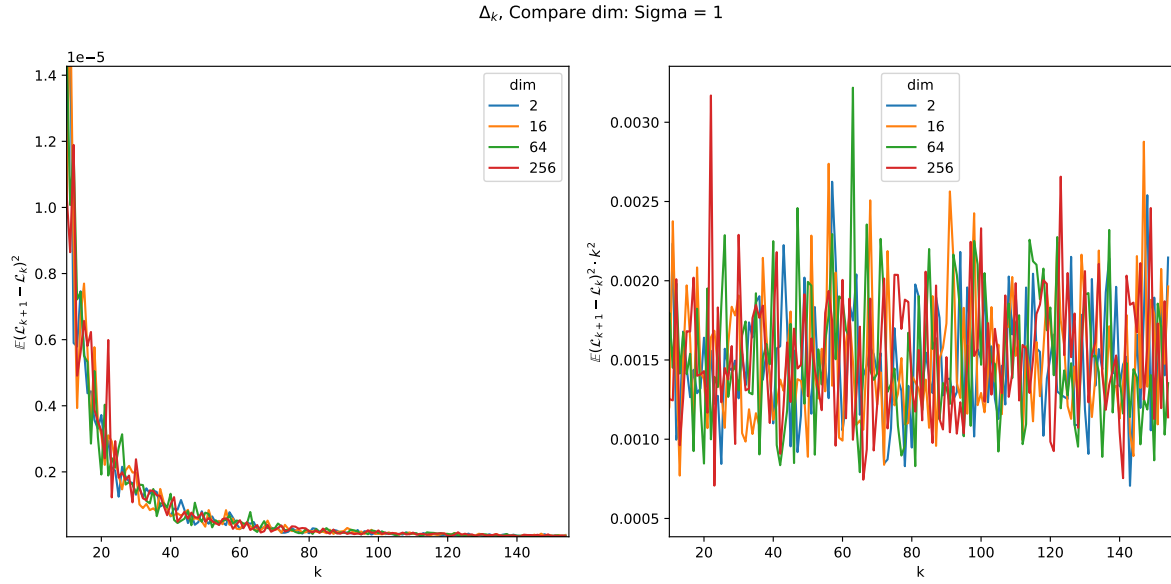


Figure 5: Delta function landscape varying the number of dimensions.

Comparing Different Subspace Dimensions Figure 5 shows that, when using random directions, increasing the projection dimension d does not significantly alter the overall shape of Δ_k . This suggests that only a few directions dominate the variation — motivating our focus on Hessian-based projections in the main experiment.

In all cases, the right-hand plots (showing $\Delta_k \cdot k^2$) exhibit a roughly $\mathcal{O}(1/k)$ decay, confirming that the incremental effect of adding one more sample diminishes proportionally to $1/k$ as the dataset grows.

The preliminary experiments show that the loss landscape indeed smooths out and becomes more stable as the training set size N increases. However, because we used random projection directions, these results capture only a generic view of stability. This observation motivates our main experiment, in which we project onto the Hessian’s top eigenvectors — i.e., the directions of greatest curvature — to obtain a more precise understanding of when and how the loss surface converges.

5.2 Moving Forward: Projection onto Dominant Hessian Eigenvectors

Projection Directions. In the main experiment, we replace random directions with the $d = 10$ eigenvectors of the Hessian at the local minimizer \mathbf{w}^* that correspond to its largest eigenvalues. Prior work [7] shows these top modes capture nearly all of the non-negligible curvature, and Figure 1 confirms a rapid eigenvalue decay. Fixing $d = 10$ balances computational cost and fidelity, and our tests on Fashion-MNIST and CIFAR demonstrate that this choice suffices even for complex architectures.

Objectives. By projecting onto these principal directions, we aim to:

- Obtain a clearer view of how the loss surface changes as k grows, since these directions drive the largest loss variations.
- Accurately identify the threshold k^* at which further data cause only negligible shifts in the local curvature.
- Empirically validate our theoretical Δ_k estimates by comparing them against Monte Carlo measurements in this eigenvector subspace.

5.2.1 Visualizing the Loss Landscape

Figures 6 and 7 display 3D plots of $\mathcal{L}_k(\boldsymbol{\theta})$ (left) and $[\mathcal{L}_{k+1}(\boldsymbol{\theta}) - \mathcal{L}_k(\boldsymbol{\theta})]^2$ (right), where $\boldsymbol{\theta}$ varies over the span of the top two Hessian eigenvectors. The procedure mirrors the random-direction case but uses these maximally informative axes.

In Figure 6 (small k , e.g. $k = 1$), the loss surface projected onto the top two Hessian eigenvectors is noticeably more structured and less erratic than in the random-direction case. This confirms that these eigenvectors capture the most influential directions of loss variation. The squared-difference plot also shows larger peaks, indicating that the model is highly sensitive to new data along these key axes when k is small.

By contrast, Figure 7 (maximum k) shows a much smoother loss surface and a greatly reduced squared-difference. As the dataset grows, the loss changes less along the principal curvature directions, and the model’s local behavior stabilizes. Notably, even at large k , the squared difference remains higher than in the random-direction experiment, providing a practical upper bound on landscape fluctuations. These findings reinforce that projecting onto the top eigenvectors effectively reveals the convergence behavior of the loss landscape and helps intuitively understand the existence of the point beyond which additional data have minimal impact.

5.2.2 Visualizing the Δ_k Function

Figure 8 presents the Monte Carlo estimate of Δ_k in the subspace spanned by the top $d = 10$ Hessian eigenvectors. Compared to the random-direction experiment, Δ_k here has a higher value — reflecting the large curvature captured by these eigenvectors. The right-hand plot of $\Delta_k \cdot k^2$ confirms an approximate $\mathcal{O}(1/k)$ convergence rate. These observations show that projecting onto the leading eigen-directions not only highlights the greatest loss sensitivity but also yields a reliable upper bound on how quickly the landscape stabilizes as more data are added.

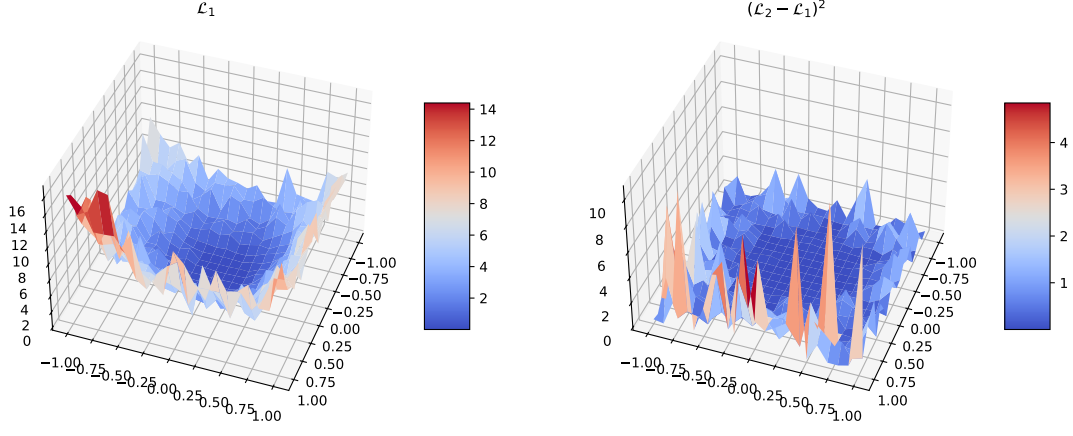


Figure 6: Loss landscape \mathcal{L}_k and squared difference for small k , projected onto the top two Hessian eigenvectors.

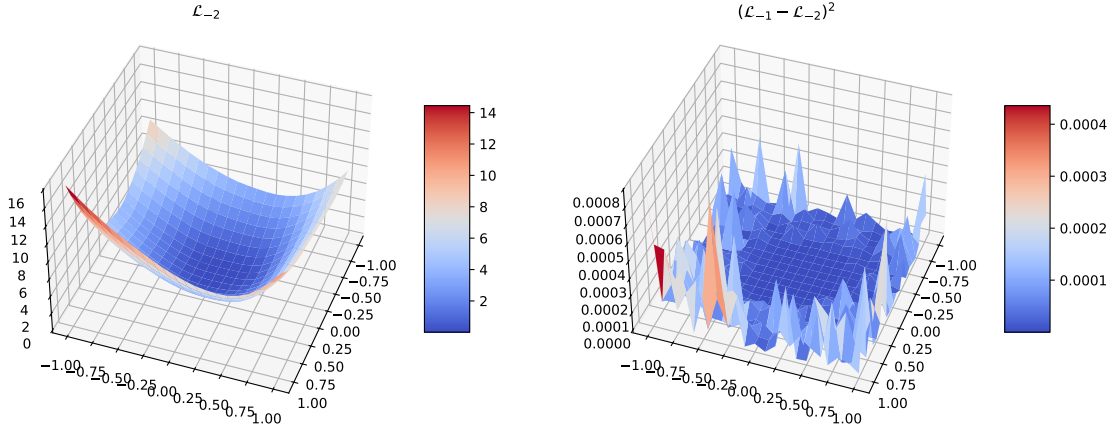


Figure 7: Loss landscape \mathcal{L}_k and squared difference for maximum k , projected onto the top two Hessian eigenvectors.

Δ_k : $\sigma = 1$, dimensions = 10, $K = 64$

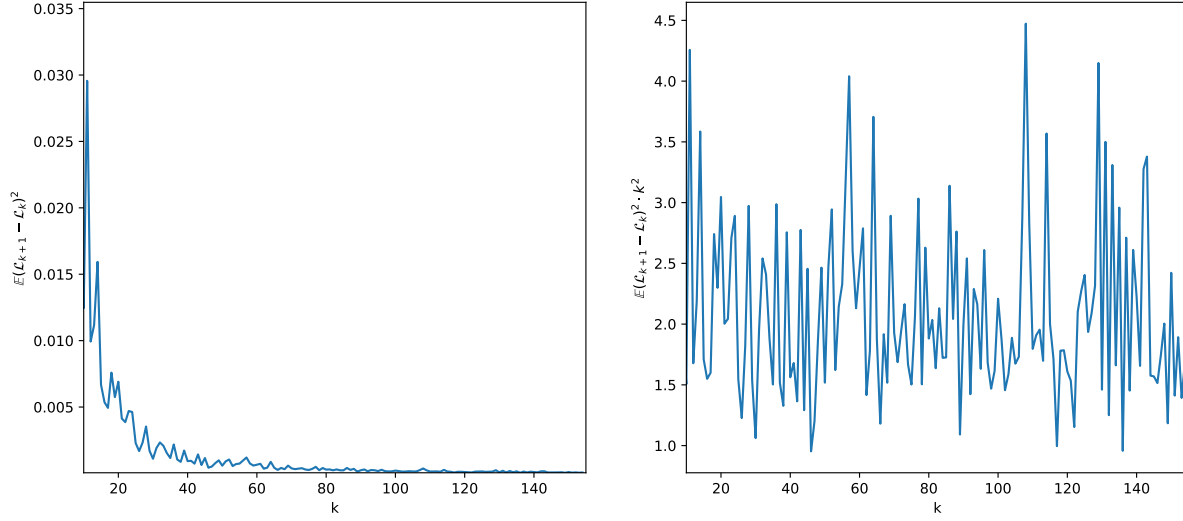


Figure 8: Delta function landscape

5.3 Main Experiment: Theoretical vs. Empirical Δ_k

In this experiment, we compare our Hessian-based theoretical estimate of Δ_k with the empirical Monte Carlo measurements.

We approximate Δ_k by

$$\Delta_k \approx \frac{\sigma^4}{4} \left(2 \sum_{i=1}^d (\lambda_{k+1}^i - \lambda_k^i)^2 + \left(\sum_{i=1}^d (\lambda_{k+1}^i - \lambda_k^i) \right)^2 \right),$$

where $\{\lambda_k^i\}_{i=1}^d$ and $\{\lambda_{k+1}^i\}_{i=1}^d$ are the top d Hessian eigenvalues at sample sizes k and $k + 1$, and σ is the perturbation variance.

1. **Model & subspace size.** Train a network to obtain \mathbf{w}^* . Choose d based on the rapid eigenvalue decay in Figure 1.
2. **Eigenvalue computation.** For each k in the range of interest (typically the largest K sizes), compute the top d eigenvalues via the power method.
3. **Theoretical Δ_k .** Plug these eigenvalues into the formula above to obtain a sequence of theoretical estimates.
4. **Empirical Δ_k .** Independently estimate Δ_k by Monte Carlo sampling of perturbations along the same top- d eigenvectors as it was in the previous experiment.
5. **Comparison.** Plot both theoretical and empirical Δ_k on the same axes to assess how tightly the theory bounds the observed values.

Figure 9 shows the theoretical estimate of Δ_k (dashed line) alongside the empirical Monte Carlo measurements (solid line). Across all values of k , the theory curve remains above the empirical one, demonstrating that our eigenvalue-based formula provides a valid upper bound for the true loss-landscape changes.

6 Discussion

The gap between the theoretical and empirical curves arises because the estimate uses only the top d eigenvalues. Therefore, focusing on the leading modes yields a reliable and efficient criterion for determining when adding more data has negligible effect on the local loss geometry.

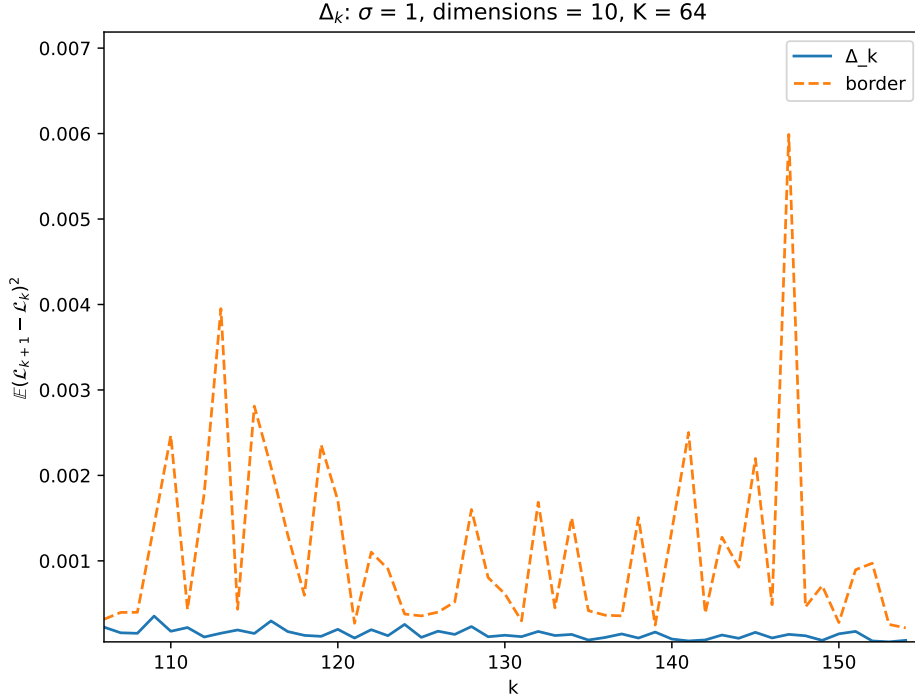


Figure 9: Delta function landscape

Our Hessian-projection framework provides a clear picture of how a neural network’s loss landscape evolves with training-set size. By restricting attention to the d principal curvature directions (the top Hessian eigenvectors), we obtain far more structured 3D loss surfaces and a sharply decaying landscape-difference measure

$$\Delta_k = \mathbb{E}_{p(\theta)} [L_{k+1}(\theta) - L_k(\theta)]^2,$$

which empirically follows an approximate $O(1/k)$ trend. Moreover, the Hessian-based bound

$$\Delta_k \approx \frac{\sigma^4}{4} \left(2 \sum_{i=1}^d (\lambda_{k+1}^i - \lambda_k^i)^2 + \left(\sum_{i=1}^d (\lambda_{k+1}^i - \lambda_k^i) \right)^2 \right)$$

consistently upper-bounds the Monte Carlo estimates (9). This confirms that only a small number of eigen-modes drive the bulk of loss-landscape change.

A practical outcome is a stopping criterion for data collection: once the leading eigenvalues and Δ_k plateau, adding more samples yields negligible changes in the loss geometry. This lets practitioners avoid unnecessary annotation and compute without sacrificing model stability.

Limitations and Future Work Our study used $d = 10$ principal directions and relatively MLPs on MNIST-like tasks. Deeper or convolutional architectures, alternative loss functions, or non-i.i.d. data may shift the spectrum decay and require reconsidering d . Extending this Hessian-based convergence criterion to large models or streaming data remains an exciting direction.

7 Conclusion

We have introduced and validated a Hessian-projection approach to identify when a neural network’s loss landscape “settles” as training data grows. By projecting onto the top eigenvectors of the Hessian, we both visualize and quantify the landscape’s sensitivity via the Δ_k function, and derive a tight

eigenvalue-difference bound that serves as a reliable upper bound on loss-landscape changes. Our results demonstrate a clear “sufficient sample size” threshold: beyond this, further data become insignificant in local curvature. This criterion provides a concrete guide for efficient dataset sizing and early stopping in model training.

References

- [1] Derya Soydaner. A comparison of optimization algorithms for deep learning. *International Journal of Pattern Recognition and Artificial Intelligence*, 34(13):2052013, April 2020. ISSN 1793-6381. doi: 10.1142/s0218001420520138. URL <http://dx.doi.org/10.1142/S0218001420520138>.
- [2] Lei Wu, Zhanxing Zhu, and Weinan E. Towards understanding generalization of deep learning: Perspective of loss landscapes. *preprint arXiv:1706.10239*, 2017. Characteristics of the loss landscape explain the good generalization capability.
- [3] Kaare Brandt Petersen and Michael Syskind Pedersen. The matrix cookbook. <https://www.math.uwaterloo.ca/~hwolkowi/matrixcookbook.pdf>, 2012. A collection of facts about matrices and matters relating to them.
- [4] Li Deng. The mnist database of handwritten digit images for machine learning research. *IEEE Signal Processing Magazine*, 29(6), 2012. URL <https://api.semanticscholar.org/CorpusID:5280072>. The database of handwritten digits.
- [5] Han Xiao, Kashif Rasul, and Roland Vollgraf. Fashion-mnist: a novel image dataset for benchmarking machine learning algorithms. *preprint arXiv:1708.07747*, 2017. A dataset of Zalando’s article images.
- [6] Nikita Kiselev and Andrey Grabovoy. Unraveling the hessian: A key to smooth convergence in loss function landscapes. *arXiv preprint arXiv:2409.11995*, 2024. Upper bounds via Hessian for fully connected neural networks.
- [7] Levent Sagun, Utku Evci, Ugur Guney, Yann Dauphin, and Leon Bottou. Empirical analysis of the hessian of over-parametrized neural networks. *preprint arXiv:1706.04454*, 2018. In over-trained neural networks the Hessian rank is often low; the active subspace may be significantly smaller.
- [8] Behrooz Ghorbani, Shankar Krishnan, and Ying Xiao. An investigation into neural net optimization via hessian eigenvalue density. In *International Conference on Machine Learning*, 2019. URL <https://proceedings.mlr.press/v97/ghorbani19b/ghorbani19b.pdf>. Observed large isolated eigenvalues in the spectrum and a surprising concentration of the gradient in the corresponding eigenspaces.
- [9] Vladislav Meshkov, Nikita Kiselev, and Andrey Grabovoy. Convnets landscape convergence: Hessian-based analysis of matricized networks, 2024. URL <https://ieeexplore.ieee.org/document/10899113>. Upper bounds via Hessian for convolutional neural networks.
- [10] Jordan Hoffmann, Sebastian Borgeaud, Arthur Mensch, Elena Buchatskaya, Trevor Cai, Eliza Rutherford, Diego de Las Casas, Lisa Anne Hendricks, Johannes Welbl, Aidan Clark, et al. Training compute-optimal large language models. *preprint arXiv:2203.15556*, 2022. Motivations behind overloaded models and the importance of optimal training size estimation.
- [11] Hao Li, Zheng Xu, Gavin Taylor, Christoph Studer, and Tom Goldstein. Visualizing the loss landscape of neural nets. *preprint arXiv:1712.09913*, 2018. Methods of visualizing loss function curvature and comparing different functions.
- [12] Olivier Bousquet and André Elisseeff. Stability and generalization. *Journal of Machine Learning Research*, 2:499–526, 2002. Submitted July 2001; Published March 2002.
- [13] André Elisseeff, Theodoros Evgeniou, and Massimiliano Pontil. Stability of randomized learning algorithms. *Journal of Machine Learning Research*, 6:55–79, 2005. Submitted February 2004; Revised August 2004; Published January 2005.

- [14] Noah Golmant, Zhewei Yao, Amir Gholami, Michael Mahoney, and Joseph Gonzalez. pytorch-hessian-eigenthings: efficient pytorch hessian eigendecomposition, October 2018. URL <https://github.com/noahgolmant/pytorch-hessian-eigenthings>.

A Appendix

A.1 Proof of Theorem 1

Proof. Starting from the second-order Taylor expansion around the local minimizer \mathbf{w}^* , we have

$$\mathcal{L}_{k+1}(\mathbf{w}) - \mathcal{L}_k(\mathbf{w}) \approx [\mathcal{L}_{k+1}(\mathbf{w}^*) - \mathcal{L}_k(\mathbf{w}^*)] + \frac{1}{2} \boldsymbol{\theta}^\top (\boldsymbol{\Lambda}_{k+1} - \boldsymbol{\Lambda}_k) \boldsymbol{\theta},$$

where $\boldsymbol{\theta} = \mathbf{P}^\top (\mathbf{w} - \mathbf{w}^*)$ and $\boldsymbol{\Lambda}_j = \mathbf{P}^\top \mathbf{H}_j(\mathbf{w}^*) \mathbf{P}$.

Let $p(\boldsymbol{\theta})$ be a distribution with mean $\mathbf{m} = \mathbb{E}[\boldsymbol{\theta}] = 0$ and covariance $\boldsymbol{\Sigma} = \mathbb{D}[\boldsymbol{\theta}]$. Denote

$$\mathbf{A} = \boldsymbol{\Lambda}_{k+1} - \boldsymbol{\Lambda}_k.$$

Then, by standard matrix-expectation results (see [3, p. 35]),

$$\mathbb{E}[\mathcal{L}_{k+1}(\mathbf{w}) - \mathcal{L}_k(\mathbf{w})] = \mathbb{E}[\frac{1}{2} \boldsymbol{\theta}^\top \mathbf{A} \boldsymbol{\theta}] = \frac{1}{2} (\text{Tr}(\mathbf{A} \boldsymbol{\Sigma}) + \mathbf{m}^\top \mathbf{A} \mathbf{m}) = \frac{1}{2} \text{Tr}(\mathbf{A} \boldsymbol{\Sigma}).$$

Similarly, using [3, p. 43],

$$\mathbb{D}[\mathcal{L}_{k+1}(\mathbf{w}) - \mathcal{L}_k(\mathbf{w})] = \frac{1}{4} \left(2 \text{Tr}(\mathbf{A}^2 \boldsymbol{\Sigma}^2) + 4 \mathbf{m}^\top \mathbf{A}^2 \mathbf{m} \sigma^2 \right) = \frac{1}{2} \sigma^4 \text{Tr}(\mathbf{A}^2),$$

where we have set $\boldsymbol{\Sigma} = \sigma^2 \mathbf{I}$ and used $\mathbf{m} = 0$.

Since

$$\Delta_k = \mathbb{D}[\mathcal{L}_{k+1} - \mathcal{L}_k] + (\mathbb{E}[\mathcal{L}_{k+1} - \mathcal{L}_k])^2,$$

we get

$$\Delta_k \approx \frac{1}{2} \sigma^4 \text{Tr}(\mathbf{A}^2) + \frac{1}{4} (\text{Tr}(\mathbf{A} \boldsymbol{\Sigma}))^2 = \frac{\sigma^4}{4} \left(2 \text{Tr}(\mathbf{A}^2) + (\text{Tr}(\mathbf{A}))^2 \right).$$

Finally, since

$$\text{Tr}(\mathbf{A}) = \sum_{i=1}^d (\lambda_{k+1}^i - \lambda_k^i), \quad \text{Tr}(\mathbf{A}^2) = \sum_{i=1}^d (\lambda_{k+1}^i - \lambda_k^i)^2,$$

we arrive at the stated approximation

$$\Delta_k \approx \frac{\sigma^4}{4} \left(2 \sum_{i=1}^d (\lambda_{k+1}^i - \lambda_k^i)^2 + \left(\sum_{i=1}^d (\lambda_{k+1}^i - \lambda_k^i) \right)^2 \right).$$

□